IEEE Access
Multidisciplinary ⋮ Rapid Review ⋮ Open Access Journal

Received 26 December 2023, accepted 6 January 2024, date of publication 11 January 2024, date of current version 23 February 2024.

Digital Object Identifier 10.1109/ACCESS.2024.3352608

RESEARCH ARTICLE

Cooling Structure Design of High-Speed Permanent Magnet Synchronous Machine With Axial Ventilation Self-Cooling Rotor

HAO LUO[1], YUE ZHANG[2], (Member, IEEE), HUIJUN WANG[3], (Member, IEEE), GUANGWEI LIU[1], (Member, IEEE), AND FENGGE ZHANG[1], (Member, IEEE)

[1]School of Electrical Engineering, Shenyang University of Technology, Shenyang 110870, China
[2]School of Electrical Engineering, Shandong University, Jinan 250100, China
[3]School of Instrumentation and Optoelectronic Engineering, Beihang University, Beijing 100083, China

Corresponding author: Huijun Wang (huijunwang_buaa@163.com)

This work was supported by the National Natural Science Foundation of China under Project 51920105011 and Project 52077121.

ABSTRACT In order to address the challenges of high loss density, difficult heat dissipation, and irreversible demagnetization in high temperature of high-speed permanent magnet machine, an innovative cooling structure with axial ventilation and self-cooling rotor is proposed to enhance temperature distribution. The cooling efficiency of the cooling structure is defined, and the influence of the rotor vent on the electromagnetic and air friction loss is analyzed. The governing equation for the fluid flow in a rotating pipe is derived from a fluid model analysis of a ventilation hole rotating at any angle to the axis of rotation. The calculated results are validated against the results obtained from computational fluid dynamics. The sensitivity of rotor cooling performance to various control factors using the variance index method. Subsequently, the cooling structure was enhanced based on the findings of the analysis. The calculation results indicate that the heat dissipation effect of the axial ventilation self-cooled rotor has decreased by 4.17 °C compared to before the improvement. The temperature rise experiment verified the accuracy of temperature calculation and the effectiveness of the cooling structure, providing strong support for the design of axial self-ventilation cooling system for high-speed machines.

INDEX TERMS Cooling structure, heat dissipation, high-speed machine, permanent magnet synchronous machine.

I. INTRODUCTION

High-speed permanent magnet synchronous machine (HSPMSM) is an attractive solution for applications such as compressors, blowers and energy storage flywheels because of their small size, high efficiency, high power density and high rotor strength [1]. However, the performance of HSPMSM is limited by their cooling systems due to the increase of volume loss density. If the cooling structure is not designed properly, the high-speed rotating rotor's heat lacks an effective heat dissipation channel, and thus relies solely on the air gap to flow to the stator. However, air has poor heat dissipation, which can result in excessive temperature rise of the rotor. Excessive rotor temperature rise can cause irreversible demagnetization of the permanent magnet, which not only affects the machine's performance but also jeopardizes the reliable operation of the permanent magnet machine [2], [3], [4]. Therefore, the cooling problem of HSPMSM has become a focus of attention.

Due to the significant thermal resistance between the rotor and the external surface of high-speed permanent magnet synchronous motors, the external cooling system of the casing often fails to meet the requirements [5]. The open-structure internal air ventilation system can directly dissipate heat

The associate editor coordinating the review of this manuscript and approving it for publication was Feifei Bu.

from the machine without incurring high cooling costs, making it widely used in industrial applications. An air cooling system with radial, axial and circumferential air ducts is proposed [6]. The air is driven by a rotating shaft and can effectively cool the internal components. Stator ventilation parameters such as vent locations, vent widths and the height of a baffle added to the stator-casing duct are optimized [7], and the peak temperature of stator windings is significantly reduced. The influence of ventilation mode on the temperature distribution is also analyzed. Compared with the PMSM with one air inlet, the maximum temperature of the PMSM with two air inlets is reduced by 9.8 °C [8].

In order to improve the cooling efficiency, the internal liquid cooling technology has been studied and developed to avoid the internal components being directly exposed to the coolant, and an indirect liquid cooling structure has been proposed [9], [10]. A self-circulating oil cooling system for hollow shaft is proposed, which can effectively enhance the heat transfer capacity of the shaft [11]. The structure of the oil circulation system is improved and the heat dissipation capacity is improved [12]. Channel cooling is considered to be an effective cooling technology, which is comparable to the traditional cooling system either as an independent method or as a secondary heat transfer path [13]. The method of adding water-cooled pipes to the teeth is studied, and the optimum diameter and number of parallel water-cooled pipes are determined, which effectively improves the heat dissipation efficiency [14]. The effects of coolant inlet temperature and flow rate on the heat transfer coefficient are examined [15]. However, for the liquid immersion cooling system, the maintenance cost is relatively high.

In addition, HSPMSM has other heat dissipation measures. For example, in order to solve the problem of serious temperature rise caused by copper loss caused by the constraint of stator slot space, a new winding indirect liquid cooling technology with heat pipe inserted in the center of stator slot is proposed [16]. The rotor temperature is reduced by installing heat sink inside the housing [17]. Recently, an integrated machine compressor with airfoil rotor is proposed [18], which has both the function of motor and the function of axial flow compressor. The rotor of motor-compressor rotates and provides electromagnetic torque and compression function at the same time. The air from the surrounding environment enters the rotor stage and is accelerated by the rotating rotor blade to achieve a high heat transfer coefficient to cool the motor. Based on the working principle of integrated motor compressor, a flux-switching permanent magnet machine with airfoil rotor is proposed [19]. At low speed, it is both motor and axial flow fan. The self-cooling characteristic of the winged rotor can be achieved without additional cooling methods, but for the high-speed machine, it will obviously increase the rotor air friction loss, so it cannot be applied directly.

To analyze the influence of cooling structure on temperature more accurately, the improved method of temperature calculation has also been studied, such as thermal network method [20], [21], [22], [23], finite element method [24], [25] and computational fluid dynamics (CFD) [26]. On the other hand, the coupling modeling and analysis of temperature field and other physical fields are analyzed, including electromagnetic and thermal bi-directional coupling method [27], [28], [29] and indirect coupling method of temperature and shell stress field [30]. The structure of axial ventilation self-cooling system is complex, and the thermal network method is not convenient to analyze the temperature distribution. Therefore, this paper provides a fluid-solid coupling CFD method to calculate the temperature distribution.

Composite rotor high-speed permanent magnet synchronous machine (CRHSPMSM) is a new type of HSPMSM with low eddy current loss and high strength. Due to the strength of the rotor, the diameter of the rotor in high-speed permanent magnet motors is usually small. The rotor of composite rotor high-speed permanent magnet synchronous machine is made of high-strength carbon fiber material magnetically loaded. The magnetic material is in a magnetic powder state without concentrated stress generation, ensuring the strength of the rotor for larger diameters. The internal space of the rotor can be used to improve the cooling efficiency of the rotor [31], [32], [33]. The literature on the existing cooling system is mainly focused on HSPMSM, but the research on CRHSPMSM is less, which is the purpose of this paper.

In this paper, taking a CRHSPMSM as the research object, the cooling structure with axial ventilation hole self-cooling rotor is proposed. The fluid model of the cooling system is constructed, and the influence of the cooling structure on the air friction loss of the machine is analyzed. Through the numerical solution of the control equation, the characteristics of air pressure distribution and rotor temperature distribution are obtained. By designing different control factors and designing orthogonal experiments, the structural parameters of the cooling system are improved, and the effectiveness of the proposed cooling enhancement method is verified by CFD simulation. Through the temperature rise experiment, the accuracy of temperature calculation and the effectiveness of cooling structure are verified, which provides strong support for the design of axial self-ventilation cooling system of high-speed machine.

II. COOLING EFFICIENCY ANALYSIS OF AXIAL VENTILATION SELF-COOLING ROTOR COOLING STRUCTURE

In order to improve the heat dissipation effect of the rotor, a 100 kW 20000r/min CRHSPMSM with axial ventilation self-cooling rotor is designed as shown in Figure 1. The parameters of the proposed machine are shown in Table 1. The rotor yoke and shaft are one unit. The material is 42CrMo. The rotor permanent magnet material of CRHSPMSM is carbon fiber-NdFeB composite. The material of the retaining sleeve is carbon fiber. The centrifugal force produced by high-speed rotation is used to make the cooling air pass through the inside of the rotor axially without changing the structure of the rotor. At the same time, the air

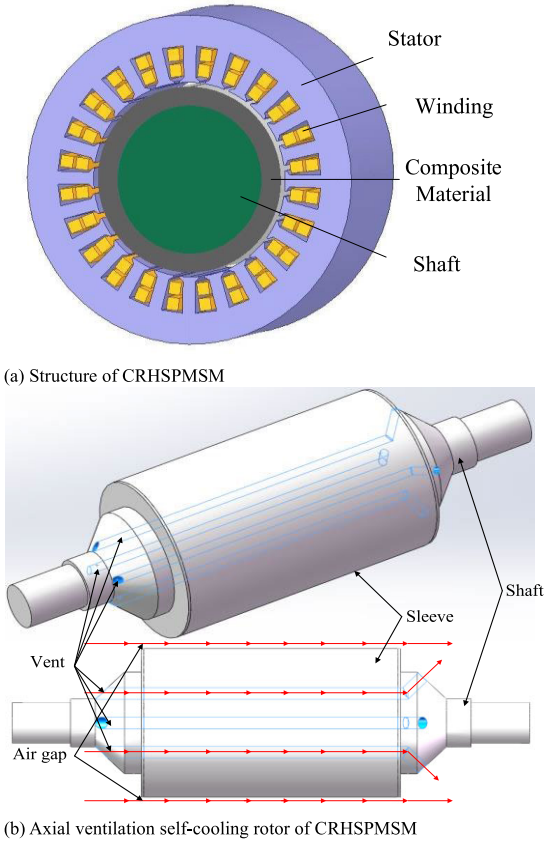

FIGURE 1. Physical model of the CRHSPMSM with axial ventilation self-cooling rotor.

TABLE 1. Parameters of the CRHSPMSM.

Parameters	Values	Parameters	Values
Rated power (kW)	100	Stator outer diameter (mm)	235
Rated speed (r/min)	20000	Stator inner diameter (mm)	132
Frequency (Hz)	666.67	rotor outer diameter (mm)	127
Number of pole-pairs	2	Axial length (mm)	195
number of slots	24	Sleeve thickness (mm)	2

flow inside the rotor and the end cavity is improved, and the cooling environment of the machine is improved. The axial vent can improve the heat dissipation condition of the machine, but it also increases the air friction loss, which is not conducive to the rotor heat dissipation, so the fluid field and temperature rise caused by air friction loss of the self-cooling rotor with the axial vent are examined.

The centrifugal hole cooling structure uses part of the mechanical power to do work on the fluid in the pipe, which increases the pressure difference between the inlet and outlet of the fluid. The input power is the external mechanical power needed to rotate the rotor after increasing the centrifugal hole, and the output power is the added value of fluid energy per unit time. The efficiency is the ratio of the two.

The input power of the cooling structure of the centrifugal hole is equal to the product of the pressure of the fluid on the wall of the centrifugal hole and the torque and speed of the viscous force relative to the rotation center. It can be obtained by the product of the torque calculated by the fluid field and the rotational speed.

$$P_1 = 2\pi nT \tag{1}$$

P_1 is the input power of the cooling structure of the centrifugal hole. n is the rotational speed. The unit is r/min. T is the torque of the fluid pressure and viscous force on the wall of the centrifugal hole to the rotation center, which is opposite to the torque of the centrifugal hole acting on the fluid.

$$T = \iint_S r \times p\mathrm{d}S + \iint_S r \times F_v\mathrm{d}S \tag{2}$$

where p is the pressure, F_v is the viscous force and r is the displacement vector of the center of rotation.

The output power P_2 of the centrifugal hole cooling system is

$$P_2 = (p_2 - p_1)\, q \tag{3}$$

where p_1 is the pressure at the entrance of the vent, p_2 is the pressure at the outlet of the centrifugal hole, and q is the flow rate.

Finally, the efficiency of the cooling structure of the centrifugal hole η can be defined as

$$\eta = \frac{P_2}{P_1} \times 100\% \tag{4}$$

The output power and efficiency of the centrifugal hole cooling structure reflect the work done by the cooling air through the ventilation hole inlet, the centrifugal hole and the vent outlet rotor and the fluid power consumption. This parameter can be used as a basis for analyzing the cooling efficiency of the centrifugal hole cooling structure.

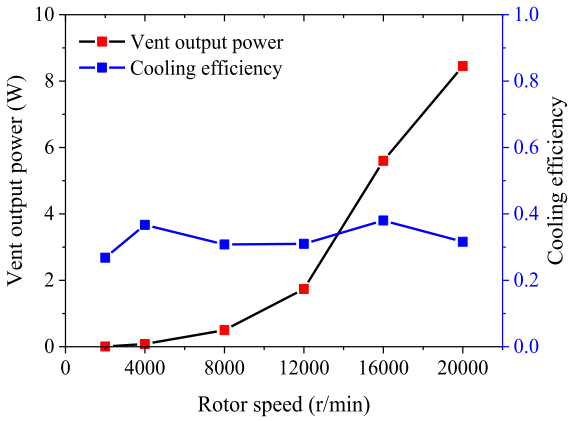

FIGURE 2. Cooling power and cooling efficiency cooling structure.

According to the calculation results in Figure 2, the output power of the centrifugal hole does not change obviously when the rotational speed is low, but when the rotational speed is

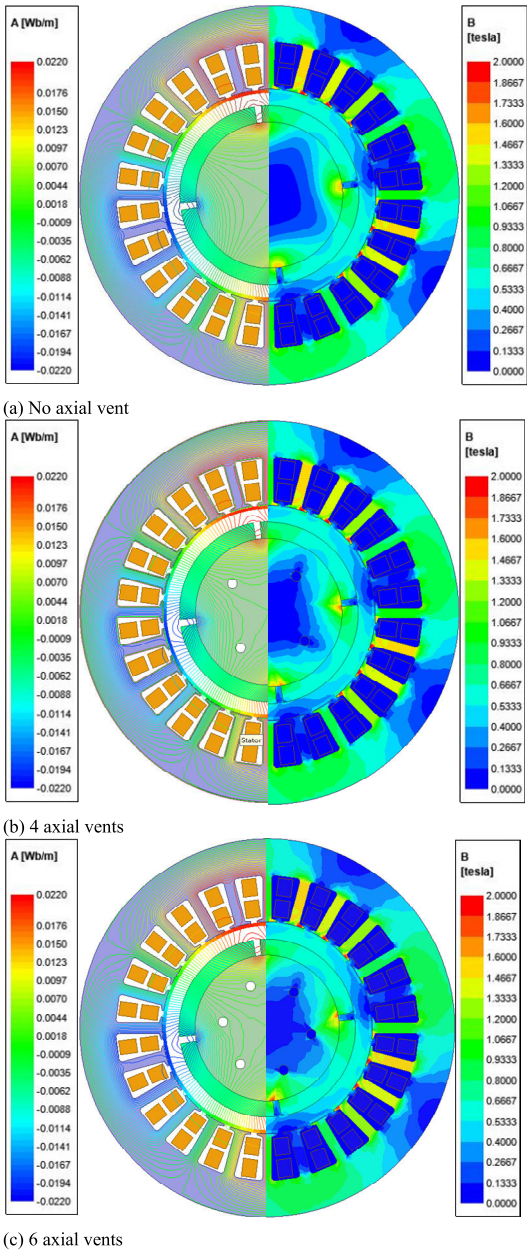

(a) No axial vent

(b) 4 axial vents

(c) 6 axial vents

FIGURE 3. Magnetic field lines and magnetic density distribution.

greater than 12000r/min, the change of power is gradually becoming apparent. Therefore, for the constant speed and low speed machine, the applicability of centrifugal hole cooling structure is poor, and this structure is more suitable for high-speed machine. The efficiency of the ventilation duct is about 32.5%, indicating that there is still much room for optimization of the centrifugal hole structure of the rotor.

III. EFFECT ON ELECTROMAGNETISM AND AIR FRICTION LOSS OF AXIAL VENTILATION HOLE

A. EFFECT ON ELECTROMAGNETISM OF AXIAL VENTILATION HOLE

In order to analyze the influence of the axial ventilation hole on the magnetic circuit of the rotor, a two-dimensional finite element model is established to analyze the transient of the machine. The parameters of the machine are shown in Table 1. 4 and 6 holes were added to the rotor yoke, with a diameter of 6mm. The magnetic force line and magnetic density cloud diagram of the rotor are shown in the Figure 3.

It can be seen that the difference in magnetic field distribution before and after adding axial ventilation ducts is very small. Therefore, the ventilation holes on the rotor yoke have almost no effect on the distribution of magnetic field lines. According to the magnetic density distribution before and after adding axial ventilation ducts, there is little change in the magnetic density distribution, so the influence of the opening on the magnetic density of the yoke is also relatively small. The back electromotive forces of the three machines at no load are 195.08V, 195.07V and 195.06V, respectively. The change is less than 0.1%, so the influence of axial opening on the electromagnetic field of the machine can be ignored.

B. EFFECT ON AIR FRICTION LOSS OF AXIAL VENTILATION HOLE

Due to the high-speed rotation of the rotor, the existence of axial ventilation holes will inevitably have a certain impact on the rotor air friction loss. In order to analyze the magnitude of this effect, a single-hole CFD model is established.

Taking the rated speed of the machine as an example, after solving the fluid finite element method, the temperature distribution cloud map and pressure distribution cloud map of the ventilation duct are obtained, as shown in Figure 4. The heat source is the heat generated by the friction between the air and the hole wall when the air flows through the ventilation hole. The k-ε turbulence model is used to calculate wall friction loss, which is added as a heat source to the ventilation hole wall. As can be seen from these two pictures, the highest temperature at the outlet of the ventilation duct is 44.15 °C. There is a temperature difference between the entrance of the ventilation duct and the outlet of the ventilation duct, which indicates that there is air friction loss and heat in the ventilation duct.

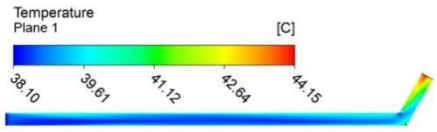

(a) Air temperature distribution in centrifugal hole

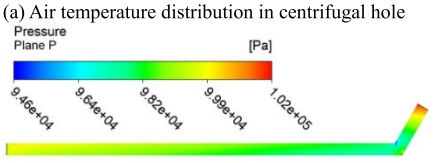

(b) Pressure distribution in centrifugal hole

FIGURE 4. Temperature and pressure distribution in centrifugal hole of 20000r/min.

According to the law of conservation of energy, the air friction loss in the ventilation duct can be calculated to be

$$p_{rwind} = cm\,(t_{\text{out}} - t_{\text{in}}) \tag{5}$$

where c is the specific heat capacity of cooling air, m is the air quality per unit time flowing through the vent, t_{out} is the average temperature at the outlet of the vent, and t_{in} is the average temperature at the entrance of the vent.

$$m = sv\rho_{air} \tag{6}$$

where s is the cross-sectional area of the vent and v is the flow speed. According to the above formula, the air friction loss of a single vent is calculated.

According to the analysis results of the influence of rotational speed on temperature field and fluid field in Figure 5, there is an exponential relationship between rotor speed and stroke friction loss of ventilation pipe. With the increase of rotor speed, the air friction loss of air in the ventilation duct increases. But for the whole, the air friction loss of a single vent in 20000r/min is only 8.5W, which is relatively small than the total loss of the machine, but has an obvious effect on the rotor with poor cooling performance.

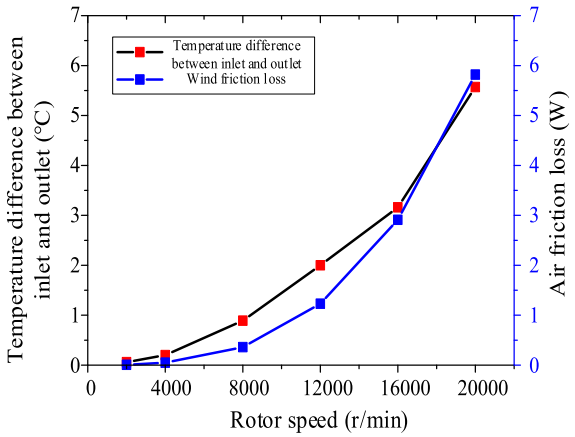

FIGURE 5. Effect of rotor speed on inlet and outlet temperature difference and air friction loss.

IV. CONTROL EQUATION OF FLUID IN ROTATING PIPE

A. VENTILATION PIPES PARALLEL TO THE AXIS OF ROTATION

The resistance caused by the friction between the air and the pipe wall caused by the viscosity of the air itself and the roughness of the pipe wall is friction resistance. The energy loss caused by overcoming friction resistance is friction resistance loss, which is referred to as the loss along the way.

When air flows in a pipe with constant interface, the loss along the way can be calculated according to the following formula.

$$\Delta P_m = \lambda \frac{1}{4R_s} \cdot \frac{\rho v^2}{2} l \tag{7}$$

where ΔP_m is the loss along the air duct, λ is the friction coefficient, v is the average air velocity in the air duct, ρ is the air density, l is the air duct length, and R_s is the air duct hydraulic radius.

$$R_s = \frac{F}{P} \tag{8}$$

where F is the cross-sectional area of the fluid part of the pipe and P is the wet perimeter that is the perimeter of the air duct in the ventilation system.

The friction resistance coefficient λ is related to the roughness of the wall of the ventilation pipe and the flow state of air in the pipe. In the rotor ventilation duct, the air flow state mostly belongs to the transition zone from the turbulent smooth zone to the rough zone. In this area, λ is calculated by the following formula

$$\frac{1}{\sqrt{\lambda}} = -2\lg\left(\frac{K}{3.7d} + \frac{2.51}{Re\sqrt{\lambda}}\right) \tag{9}$$

where K is the roughness of the inner wall of the air duct mm, Re is Reynolds number.

$$Re = \frac{v \cdot d}{\gamma} \tag{10}$$

where γ is the kinematic viscosity coefficient of the fluid.

Re is usually used as the basis for judging the state of air flow. The flow state is laminar flow when $Re \leq 2300$ and the flow state is turbulent flow when $Re > 2300$.

Figure 6 shows a model for the flow of heated air in an axially rotating ventilation duct when a uniform heat flux density q_w is applied to the pipe wall.

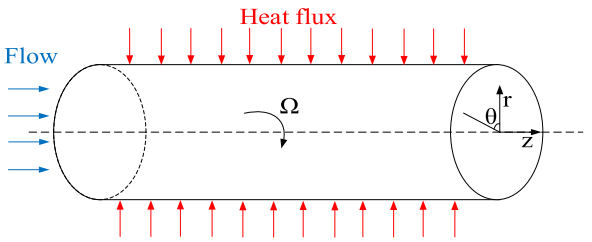

FIGURE 6. Schematic diagram of fluid computing domain.

Under the condition of rated speed, $Re > 2300$ is turbulent, and constant heat flux is applied to the pipe wall as the thermal boundary condition [34]. Assuming that the fluid parameters are constant, the viscous loss is ignored. The dimensionless temperature is defined as follows

$$\Theta = \left(T_w(z) - T(r, z, \theta, t)\right)/T_r \tag{11}$$

where T_w is defined as the average wall temperature and T_r is the reference temperature.

$$T_r = \frac{q_w}{\rho C_p v_b} \tag{12}$$

C_p is the constant pressure specific heat capacity, and v_b is the bulk velocity.

According to the hydrodynamic energy equation, the rate of change of the internal energy of a fluid micromass is equal to the sum of the net heat flow into the micromass and the power of the work done by the bulk and surface forces on the fluid micromass.

$$\frac{\partial \bar{\Theta}}{\partial t} + \frac{1}{r}\frac{\partial}{\partial r}\left(\bar{q}_r\bar{\Theta}\right) + \frac{1}{r}\frac{\partial}{\partial \theta}\left(\bar{q}_\theta\bar{\Theta}\right) + \frac{\partial}{\partial z}\left(\bar{q}_z\bar{\Theta}\right) - \bar{q}_z\frac{\partial}{\partial z}\left(\frac{\bar{T}_b}{T_r}\right)$$

$$= \frac{1}{Pe}\left[\frac{1}{r}\frac{\partial}{\partial r}\left(\bar{\alpha}_t r\frac{\partial\bar{\Theta}}{\partial r}\right)+\frac{1}{r^2}\frac{\partial}{\partial\theta}\left(\bar{\alpha}_t\frac{\partial\bar{\Theta}}{\partial\theta}\right)+\frac{\partial}{\partial z}\left(\bar{\alpha}_t\frac{\partial\bar{\Theta}}{\partial z}\right)\right] \tag{13}$$

The average heat flow in each direction $q_r = r \cdot v_r$, $q_\theta = r \cdot v_\theta$, and $q_z = r \cdot v_z$. The ratio of r to velocity in each direction is equal to the ratio of the pipe radius R to the central flow line velocity v_{cl} of the incompressible viscous laminar flow of the pipe. Peclet number $P_e = Re_p Pr$, where $Re_p = v_{cl}R/\nu$. ν is the dynamic viscosity.

The average pressure gradient in the equation for the flow component in each direction is the body velocity constant. The heating condition applied to the wall surface represents a linear increase in the instream temperature T_b in the flow direction. For a fully developed flow line, the following equation is satisfied

$$\frac{\partial T}{\partial z} = \frac{\partial T_b}{\partial z} = \frac{2q_w}{\rho C_p U_b} \tag{14}$$

B. VENTILATION PIPE ROTATING AROUND ANY AXIS

The centrifugal ventilation hole is composed of two parts, one is the ventilation hole parallel to the rotation axis, and the other is the centrifugal hole which has a certain angle with the rotation axis. The vent parallel to the axis of rotation has been analyzed previously, and the fluid model of the vent which rotates at a certain angle to the axis of rotation is analyzed in this section.

When the pipe rotates around any axis, the axial velocity distribution in the pipe changes, the secondary flow occurs on the cross section, and the convective heat transfer characteristics of the pipe will change. In this chapter, the flow and heat transfer in a circular cross-section pipe rotating around an arbitrary axis are numerically simulated. The convective heat transfer characteristics in a rotating pipe around an arbitrary axis are mainly determined by Reynolds number Re, Rossby number Ro, Prandtl number Pr and the angle α between the rotation axis and the pipe axis.

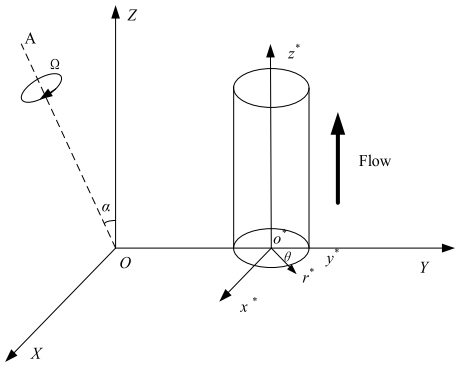

FIGURE 7. Fluid calculation domain of ventilation pipe rotating around any axis.

In Figure 7, o^*z^* is the pipeline axis, the pipe rotates around the OA, the rotation speed is Ω, the angle between the pipe axis and the rotation axis is α, the relative coordinate system (r^*, θ, z^*) is established, and the velocity component in the direction of the relative coordinate system (r^*, θ, z^*) is $u^*v^*w^*$. The diameter of the pipe is d. It is assumed that the flow field and temperature field of the pipeline are fully developed, the wall heat flux q_w is constant, and the wall temperature T_w remains constant along the circumferential direction of the section. Converting parameters to dimensionless numbers as follow:

$$\begin{aligned} r &= r^*/d \\ z &= z^*/d \\ (u, v, w) &= \left(u^*, v^*, w^*\right)/d \\ \Theta &= (T_w - T)\,T_s \\ P &= P^*/\rho W_m^{*2} \\ Ro &= W_m^*/\Omega d \\ Re &= W_m^* d/\nu \\ Pr &= \nu/\lambda \end{aligned} \tag{15}$$

where P^* is an axial pressure gradient, and T_s is the characteristic temperature.

$$\begin{aligned} P^* = p^* &- \rho\left(r\sin\theta\cos\alpha + z\sin\alpha\right)^2\Omega^2/2 \\ &- \rho\left(L + r\sin\theta\right)^2\Omega^2/2 \end{aligned} \tag{16}$$

$$T_s = q_w d/k \tag{17}$$

where k is the thermal conductivity.

It is deduced that the control equation in the relative coordinate system is

$$\begin{cases} \dfrac{\partial}{\partial r}(ru) + \dfrac{\partial v}{\partial\theta} = 0 \\ u\dfrac{\partial u}{\partial r} + \dfrac{v}{r}\dfrac{\partial u}{\partial\theta} - \dfrac{v^2}{r} \\ \quad = -\dfrac{\partial P}{\partial r} - \dfrac{2}{Ro}\left(v\cos\alpha + w\sin\alpha\cos\theta\right) \\ \quad + \dfrac{1}{Re}\left(\nabla^2 u - \dfrac{u}{r^2} - \dfrac{2}{r^2}\dfrac{\partial v}{\partial\theta}\right) \\ u\dfrac{\partial v}{\partial r} + \dfrac{v}{r}\dfrac{\partial v}{\partial\theta} - \dfrac{uv}{r} = -\dfrac{\partial P}{r\partial\theta} + \dfrac{2}{Ro}\left(u\cos\alpha + w\sin\alpha\cos\theta\right) \\ \quad + \dfrac{1}{Re}\left(\nabla^2 u - \dfrac{v}{r^2} + \dfrac{2}{r^2}\dfrac{\partial u}{\partial\theta}\right) \\ u\dfrac{\partial w}{\partial r} + \dfrac{v}{r}\dfrac{\partial w}{\partial\theta} = -\dfrac{\partial P}{\partial z} + \dfrac{2}{Ro}\left(u\cos\theta - v\sin\theta\right)\sin\alpha \\ \quad + \dfrac{1}{Re}\nabla^2 w \\ Pr\left(u\dfrac{\partial\Theta}{\partial r} + \dfrac{v}{r}\dfrac{\partial\Theta}{\partial\theta}\right) - \dfrac{4w}{Re} = \dfrac{1}{Re}\nabla^2\Theta \end{cases} \tag{18}$$

According to the above analysis and calculation, the results of the fluid field when the ventilation duct rotates around any axis are obtained. Figure 8 (a) (b) shows a rotating pipeline with the length of 50mm, the inner diameter of 8mm, and the inclination angle α of 30°, the variation of the average air flow rate and inlet/outlet pressure difference in the pipeline with rotational speed. Figure 8 (c) (d) shows the variation of the average air flow velocity and inlet/outlet pressure in the same

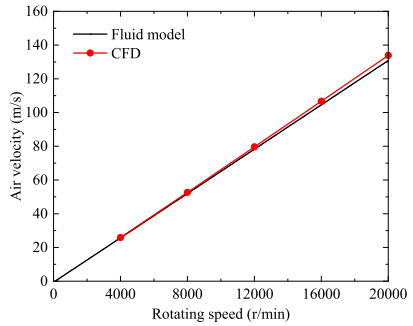

(a) Effect of rotational speed on air velocity

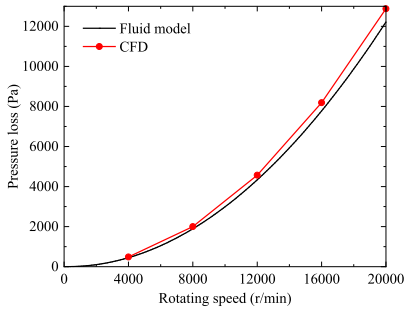

(b) Effect of rotational speed on pressure loss

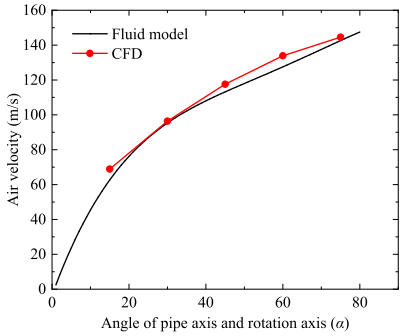

(c) Effect of the included angle on air velocity

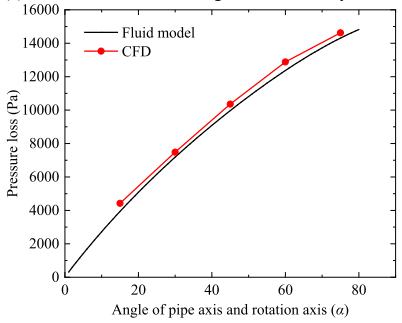

(d) Effect of the included angle on pressure loss

FIGURE 8. Effect of rotational speed and angle on fluid field.

pipeline speed of 20000r/min calculated separately by using fluid models and CFD. The angle has been increased from 0° to 90°. Calculate flow velocity and inlet/outlet pressure difference separately using fluid model and CFD. The proposed fluid calculation model results are basically consistent with the CFX model results, verifying the feasibility of the axial ventilation self-cooling structure and providing a theoretical basis for the design of the cooling structure.

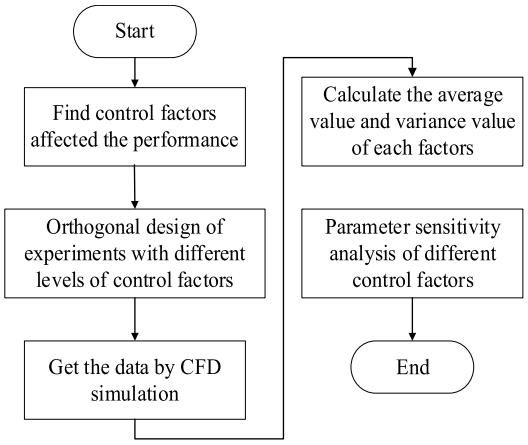

FIGURE 9. Flow chart of design method.

V. DESIGN OF COOLING STRUCTURE

When the axial rotating pipe is connected in series with the rotating pipe around any axis, the fluid velocity after series is

$$V = \frac{Q_1 + Q_2}{\pi\,(d/2)^2} = \frac{Q}{\pi\,(d/2)^2} \tag{19}$$

Q_1 is the air flow in the parallel ventilation duct, Q_2 is the air flow in the oblique air duct, and Q is the total flow.

The heat generated from the rotor to the vent air can be expressed as

$$\Phi = \frac{T_{\mathrm{r}} - T_{\mathrm{air}}}{R_{\mathrm{th}}} = hA\,(T_{\mathrm{r}} - T_{\mathrm{air}}) \tag{20}$$

where Φ is the heat generated by the rotor, R_{th} is the thermal resistance between the rotor and the fluid, T_{r} is the rotor temperature, T_{air} is the cooling air temperature, h is the thermal convection coefficient, A is the heat transfer area, which can be expressed as

$$A = l_p \pi d \tag{21}$$

L_{p} is the length of ventilation pipe.

According to Dittus-Boelter formula, for cooling fluid, the forced convection coefficient is

$$\mathrm{Nu} = 0.0023 Re^{0.8}\,\mathrm{Pr}^{0.4} \tag{22}$$

The thermal convection coefficient h is

$$h = 0.023 \left(\frac{4Q}{v\pi d}\right)^{0.8} \left(\frac{\mu C_p}{\lambda}\right)^{0.4} \frac{\lambda}{d} \tag{23}$$

The heat dissipation efficiency of ventilation pipe η can be expressed as

$$\eta = hA = 0.023 \left(\frac{4Q}{v\pi d}\right)^{0.8} \left(\frac{\mu C_p}{\lambda}\right)^{0.4} \frac{\lambda \pi d}{4} \tag{24}$$

It can be seen that η is a function of the flow rate Q and the diameter of the ventilation duct d.

In order to obtain the best cooling structure, Taguchi method is used to improve the design efficiency of ventilation parameters. The design based on orthogonal array can greatly

TABLE 2. Different levels of control factors.

Control factors	Level 1	Level 2	Level 3	Level 4
ventilation duct number N	3	4	5	6
diameter of ventilation pipe d(mm)	3	4	5	6
angle α(°)	30	45	60	75

TABLE 3. Calculation results of L16 orthogonal matrix.

Control factors			Results		
N	d(mm)	α(°)	Tr (°C)	ΔP (Pa)	V (m/s)
3	3	30	61.80	321	9.33
3	4	45	60.70	357	9.96
3	5	60	59.01	514	10.28
3	6	75	58.33	416	10.45
4	3	45	60.72	618	9.32
4	4	30	59.71	231	9.84
4	5	75	58.62	637	10.83
4	6	60	57.21	339	11.39
5	3	60	60.32	957	9.59
5	4	75	58.98	877	10.50
5	5	30	57.21	152	10.46
5	6	45	56.27	84	11.54
6	3	75	60.14	1105	10.01
6	4	60	58.24	825	10.57
6	5	45	56.71	163	11.40
6	6	30	55.53	206	12.21

reduce the experimental cost and time consumption. The design flow chart is shown in Figure 9.

In order to better verify the performance of the ventilation duct, a four-level three-factor L16 orthogonal array is designed for numerical experiments, as shown in Table 2. According to the analysis presented in Chapter 3, the increase in ventilation ducts will double the air friction loss. At the same time, considering the processing complexity, the selection range of the number of ventilation ducts is less than 6. In order to ensure the comparison of control factors under the same conditions, different ventilation duct number N, diameter of ventilation pipe d and angle α are designed under the same four levels. Each ventilation hole is guaranteed to be equally spatially distant.

The calculation results of CFD and orthogonal array are used to simulate the maximum temperature of the rotor. The calculation results of the L16 orthogonal matrix are shown in Table 3. For the traditional design method, all the simulation results need to change with the level of each factor and require 64 analyses of time. However, for the L16 orthogonal matrix, only 16 times are calculated. Obviously, the efficiency of the optimized design experiment is improved by 75%.

TABLE 4. Average value of 3 control factors under each level.

Control factors	Level	Tr (°C)	ΔP (Pa)	V (m/s)
N	3	59.96	402.00	10.01
	4	59.07	456.25	10.35
	5	58.20	517.50	10.52
	6	57.66	574.75	11.05
d(mm)	3	60.75	750.25	9.56
	4	59.41	572.5	10.22
	5	57.89	366.5	11.74
	6	56.84	261.25	11.40
α(°)	30	58.56	227.5	10.46
	45	58.60	305.5	10.56
	60	58.70	658.75	10.46
	75	59.02	758.75	10.45

Two evaluation indexes, mean $\bar{M}$ and variance SS, are used to analyze the results of the orthogonal array, and the final optimal solution is given. The definition of $\bar{M}$ and SS are as follows

$$\bar{M} = \frac{1}{m}\sum_{i=1}^{m} M_i \tag{25}$$

$$SS = \frac{1}{m}\sum_{i=1}^{m} \left(M_i - \bar{M}\right) \tag{26}$$

The average values of three kinds of control factors of different rotor ventilation structures are calculated by equation (22). The results are shown in Table 4.

In order to further optimize the optimal combination of different rotor ventilation structures, the influence of various control factors on different rotor ventilation structures at their corresponding levels is shown in Figure 10. A1-A4, B1-B4, and C1-C4 represent four levels of ventilation duct quantity N, ventilation duct diameter d, and angle α, respectively. As can be seen from Figure 10, with the increase of N and d, the maximum temperature of permanent magnet decreases significantly, and the rotor temperature increases slightly with the increase of α, but the effect is small. The sensitivity of rotor temperature, pipe pressure difference and flow velocity to these three structural parameters is different.

The sensitivity of rotor cooling performance to different control factors is analyzed by using variance index. The results are shown in Table 5. As shown in Figure 11, the diameter of ventilation duct d plays a major role in rotor cooling, accounting for about 58.5%, followed by the number of cooling ventilation ducts N, the influence accounts for 34.5%, and the influence of α is the least, accounting for about 7%. For the pressure difference between the inlet and outlet of ventilation ducts, the effects of α and d are more

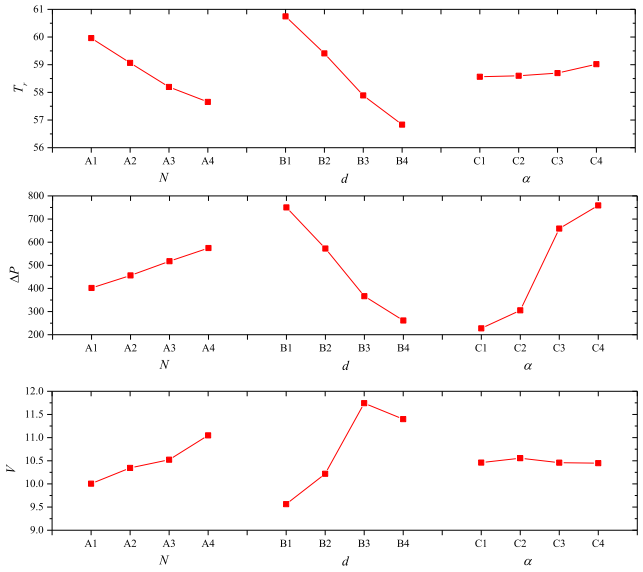

FIGURE 10. Control factors influence on the performance of cooling system.

TABLE 5. Sensitivity analysis of control factor.

Control factors		N	d	α
Tr	SS	0.876	1.485	0.179
	PC	0.345	0.585	0.07
ΔP	SS	64.81	188.5	225.6
	PC	0.135	0.394	0.471
V	SS	0.377	0.88	0.043
	PC	0.29	0.677	0.033

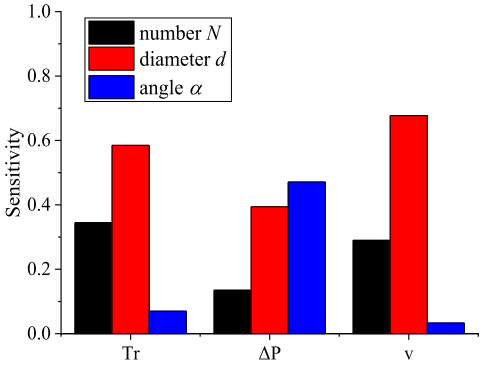

FIGURE 11. Factor influence on the performance of cooling system.

significant, accounting for 47.1% and 39.4%, respectively, and the proportion of the number of ventilation ducts N is 13.5%. For air velocity, the greatest impact is also the diameter of ventilation duct d, accounting for 67.7%, the number of cooling ventilation N, the influence accounts for 29%, and the effect of α is almost negligible, accounting for about 3.3%.

The analysis results show that with the increase of the number of ventilation pipes N and pipe diameter d, the fluid velocity increases, the turbulence intensifies, and the heat dissipation capacity of the cooling system increases. But at the same time, under the condition of constant flow rate, the

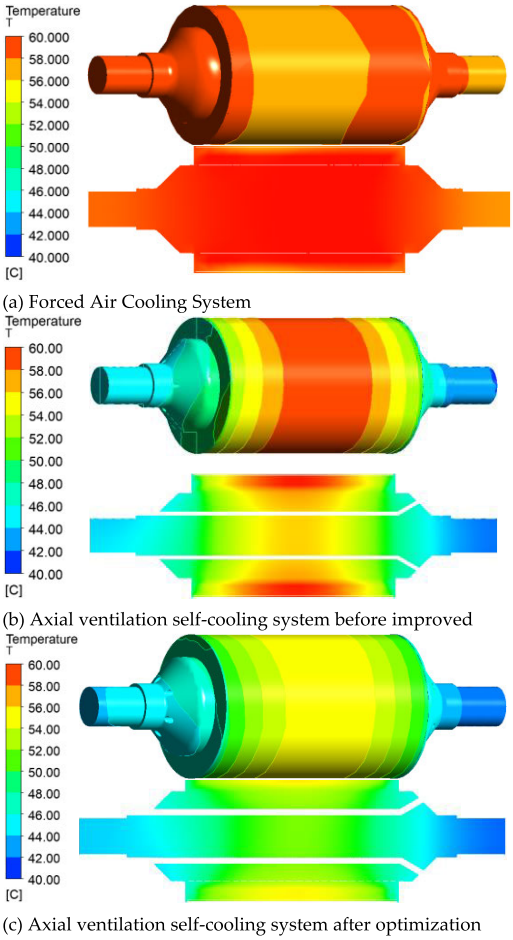

FIGURE 12. Comparison of temperature distribution.

increase of ventilation duct transportation will lead to the pressure loss and power increase of the cooling system.

Considering the sensitivity of control factors and the improvement of rotor temperature distribution, the combination of the highest rotor temperature and pressure loss is (A4B4C1). The rotor temperature calculation model of forced air cooling system, axial ventilation self-cooling system before and after improved is established, while ensuring a volumetric flow rate of 2.071×10^{-3} m^3/s for the cooling air. Figure 12 is the temperature distribution when the load is 47.75Nm and the speed is 20000r/min. Compared to forced air cooling system, the axial ventilation self-cooling system can effectively lower the rotor temperature. The improved design shows that the maximum temperature of the rotor is 55.54 °C. Compared with the initial structure, the maximum temperature of the rotor decreased by 4.17 °C. After the improvement, the cooling efficiency of the cooling system has increased from 31.6% to 36.2% based on the calculation method described in Chapter 2.

The axial ventilation duct can enhance the heat transfer of the rotor for two reasons: one is that the surface of the ventilation duct increases the heat transfer area of the wall; the other is that the axial air flow caused by centrifugal force

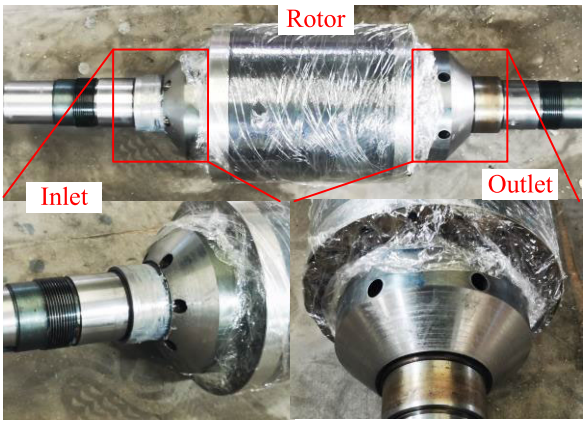

(a) Axial ventilation self-cooling rotor

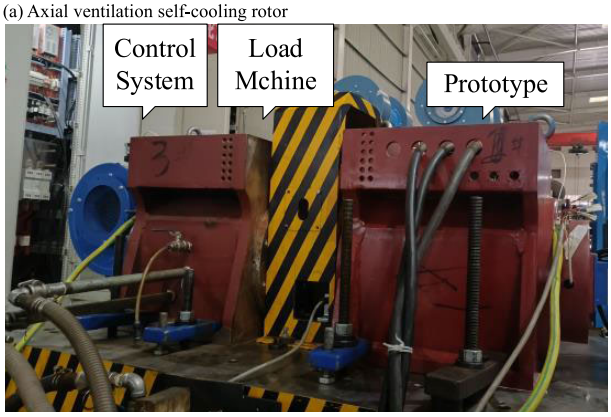

(b) Prototype and Experimental platform

FIGURE 13. Prototype and its rotor.

improves the convective heat transfer and enhances the heat transfer effect. For CRHSPMSM, the diameter of ventilation duct has the most significant effect on rotor temperature, followed by the number of ventilation ducts. As for the pressure loss, the inclination angle of the pipe and the diameter of the ventilation duct have obvious influence.

VI. EXPERIMENTAL VERIFICATION

In order to verify the effectiveness of the cooling system and the accuracy of temperature calculation, based on the axial ventilation duct self-cooling system, a prototype and a self-cooling rotor with axial ventilation are made as shown in the Figure13(a). The testing platform for the motor is shown in Figure 13(b). The prototype controls torque through the upper computer of the control system. A 100kW 20000r/min machine provides the load. The parameters of the prototype are the same as those in Table 1. The rotor permanent magnet material of CRHSPMSM is carbon fiber-NdFeB composite.

The winding temperature is measured directly by a thermistor pt100 pre-embedded in the winding coil. Winding temperature measurement is used to determine whether the temperature rise is stable and verify the accuracy of temperature calculation. Because the temperature rise of the rotor rotating at high speed is difficult to be obtained by direct measurement, this paper indirectly measures the temperature

TABLE 6. Sensitivity analysis of control factor.

Temperature rise	Stator Winding (°C)		Permanent magnet material (°C)	
	Without hole	With hole	Without hole	With hole
Experimental results	39	36	40	34
Calculation result	41.26	38.25	41.91	35.54

rise of the rotor by using the temperature characteristics of permanent magnet materials. In the stable state, the decrease in the back electromotive force of the machine is caused by demagnetization caused by the temperature rise of the permanent magnet. If the temperature change of the machine does not exceed 2 °C within 1 hour, the machine is in a thermally stable state. At this moment, the rotor load immediately decreases to 0, and the no-load back EMF is obtained by measuring the winding voltage. The no-load back EMF E_0 is

$$E_0 = 4fk_{dp}k_{NM}N\phi_{\delta 0} \tag{27}$$

For the same machine, the number of turns in series per phase N, winding coefficient k_{dp} and waveform coefficient k_{NM} are unchanged. The air gap flux $\phi_{\delta 0}$ provided by the permanent magnet under no load is

$$\phi_{\delta 0} = \frac{b_{m0}B_rA_m}{\sigma_0} \tag{28}$$

b_{m0} is the magnetic density unit of the no-load working point of the permanent magnet, A_{m} provides the cross-sectional area of flux per pole for the permanent magnet, σ_0 is the no-load magnetic leakage coefficient of the permanent magnet, and B_{r} is the remanence of the permanent magnet material.

The no-load back EMF of the same machine is proportional to the remanence of the permanent magnet material at the same working frequency. Due to the increase of temperature, the magnetic properties of permanent magnet materials are weakened, and the residual magnetic induction intensity B_{r1} of permanent magnet at temperature t_1 is

$$B_{r1} = B_{r0}\left(1 - \frac{IL}{100}\right)\left[1 - \frac{\alpha_{Br}}{100}(t_1 - t_0)\right] \tag{29}$$

α_{Br} is the temperature coefficient of permanent magnet material, IL is the irreversible loss coefficient of permanent magnet material, and B_{r0} is the remanence of permanent magnet material at temperature t_0. According to formula 29, the temperature of rotor permanent magnet material can be obtained by measuring no-load back EMF.

The temperature rise experiment was conducted under two conditions: with the vent open and with the vent blocked. When the rotor speed is 20000r/min, the experimental and calculated results of the temperature of the winding and permanent magnet material are shown in Table 6. According to the results, the stator winding temperature decreased by 3 °C and the rotor temperature decreased by 6 °C. The errors between the calculated results and the experimental results of

stator winding temperature and permanent magnet material temperature are 6.3% and 4.5%, respectively. The calculation error meets the actual requirement of calculation accuracy. The experimental results verify the accuracy of temperature rise calculation and the effectiveness of cooling structure, and provide strong support for the design of axial self-ventilation cooling system of high-speed machine.

VII. CONCLUSION

This paper proposes an axial ventilation self-cooling rotor structure based on a CRHSPMSM. The structure makes use of the centrifugal force produced by high-speed rotation to make the cooling air axially pass through the interior of the rotor and improve the cooling environment of the machine. The cooling efficiency of the cooling structure is analyzed and the governing equation of the rotating pipe fluid is established. The variables affecting the cooling performance are found out. According to different control factors, the orthogonal experiment is designed. The data are obtained by CFD simulation, the influence ratio of each variable at different levels is calculated, and the parameter sensitivity of the control variable is analyzed. The calculation results show that the heat dissipation effect of the axial ventilation self-cooled rotor has decreased by 4.17 °C after improvement, and the cooling efficiency of the cooling system has increased by 4.6%. This paper provides a reference for the design of high-speed machine with axial ventilation self-cooling structure.

REFERENCES

[1] D. Gerada, A. Mebarki, N. L. Brown, C. Gerada, A. Cavagnino, and A. Boglietti, "High-speed electrical machines: Technologies, trends, and developments," *IEEE Trans. Ind. Electron.*, vol. 61, no. 6, pp. 2946–2959, Jun. 2014, doi: 10.1109/TIE.2013.2286777.

[2] T. Han, Y. Wang, and J.-X. Shen, "Analysis and experiment method of influence of retaining sleeve structures and materials on rotor eddy current loss in high-speed PM motors," *IEEE Trans. Ind. Appl.*, vol. 56, no. 5, pp. 4889–4895, Sep. 2020, doi: 10.1109/TIA.2020.3009909.

[3] W. Yu, W. Hua, and Z. Zhang, "Cooling analysis of high-speed stator-permanent magnet flux-switching machines for fuel-cell electric vehicle compressor," *IEEE Trans. Veh. Technol.*, vol. 71, no. 1, pp. 210–219, Jan. 2022, doi: 10.1109/TVT.2021.3126108.

[4] H. Fang, D. Li, R. Qu, J. Li, C. Wang, and B. Song, "Rotor design and eddy-current loss suppression for high-speed machines with a solid-PM rotor," *IEEE Trans. Ind. Appl.*, vol. 55, no. 1, pp. 448–457, Jan. 2019, doi: 10.1109/TIA.2018.2871095.

[5] N. V. Korovkin, D. Verkhovtsev, and S. Gulay, "Rotor air-cooling efficiency of powerful turbogenerator," *IEEE Trans. Energy Convers.*, vol. 36, no. 3, pp. 1983–1990, Sep. 2021, doi: 10.1109/TEC.2020.3045063.

[6] P. Asef, R. B. Perpina, and M. R. Barzegaran, "An innovative natural air-cooling system technique for temperature-rise suppression on the permanent magnet synchronous machines," *Electric Power Syst. Res.*, vol. 154, pp. 174–181, Jan. 2018, doi: 10.1016/j.epsr.2017.07.031.

[7] K. Bersch, S. Nuzzo, P. H. Connor, C. N. Eastwick, R. Rolston, and M. Galea, "Thermal and electromagnetic stator vent design optimisation for synchronous generators," *IEEE Trans. Energy Convers.*, vol. 36, no. 1, pp. 207–217, Mar. 2021, doi: 10.1109/TEC.2020.3004393.

[8] L. Wang, Y. Li, B. Kou, F. Marignetti, and A. Boglietti, "Influence of ventilation modes on the 3D global heat transfer of PMSM based on polyhedral mesh," *IEEE Trans. Energy Convers.*, vol. 37, no. 2, pp. 1455–1466, Jun. 2022, doi: 10.1109/TEC.2021.3137672.

[9] L. Li, S. Niu, S. L. Ho, W. N. Fu, and Y. Li, "A novel approach to investigate the hot-spot temperature rise in power transformers," *IEEE Trans. Magn.*, vol. 51, no. 3, pp. 1–4, Mar. 2015, doi: 10.1109/TMAG.2014.2359956.

[10] R. Camilleri, P. Beard, D. A. Howey, and M. D. McCulloch, "Prediction and measurement of the heat transfer coefficient in a direct oil-cooled electrical machine with segmented stator," *IEEE Trans. Ind. Electron.*, vol. 65, no. 1, pp. 94–102, Jan. 2018, doi: 10.1109/TIE.2017.2714131.

[11] Y. Zhou, H. Xu, Q. Xiong, X.-J. Niu, and R.-G. Xie, "Design, performance analysis, and testing of composite components for the oil-cooling air-core stator of a high temperature superconducting motor," *IEEE Trans. Appl. Supercond.*, vol. 31, no. 8, pp. 1–5, Nov. 2021, doi: 10.1109/TASC.2021.3101754.

[12] G. Zhu, L. Li, Y. Mei, T. Liu, and M. Xue, "Design and analysis of a self-circulated oil cooling system enclosed in hollow shafts for axial-flux PMSMs," *IEEE Trans. Veh. Technol.*, vol. 71, no. 5, pp. 4879–4888, May 2022, doi: 10.1109/TVT.2022.3154150.

[13] F. Zhang, D. Gerada, Z. Xu, X. Zhang, H. Zhang, C. Gerada, M. Zhu, L. Xia, W. Zhang, and M. Degano, "Improved thermal modeling and experimental validation of oil-flooded high-performance machines with slot-channel cooling," *IEEE Trans. Transport. Electrific.*, vol. 8, no. 1, pp. 312–324, Mar. 2022, doi: 10.1109/TTE.2021.3106819.

[14] J. Chang, Y. Fan, J. Wu, and B. Zhu, "A yokeless and segmented armature axial flux machine with novel cooling system for in-wheel traction applications," *IEEE Trans. Ind. Electron.*, vol. 68, no. 5, pp. 4131–4140, May 2021, doi: 10.1109/TIE.2020.2982093.

[15] S. T. Lundmark, E. A. Grunditz, T. Thiringer, A. Andreasson, A. Bergqvist, R. Orbay, and E. Jansson, "Heat transfer coefficients in a coupled 3-D model of a liquid-cooled IPM traction motor compared with measurements," *IEEE Trans. Ind. Appl.*, vol. 57, no. 5, pp. 4805–4814, Sep. 2021, doi: 10.1109/TIA.2021.3095242.

[16] W. Geng, T. Zhu, Q. Li, and Z. Zhang, "Windings indirect liquid cooling method for a compact outer-rotor PM starter/generator with concentrated windings," *IEEE Trans. Energy Convers.*, vol. 36, no. 4, pp. 3282–3293, Dec. 2021, doi: 10.1109/TEC.2021.3084507.

[17] W. Le, M. Lin, K. Lin, L. Jia, and S. Wang, "A rotor cooling enhanced method for axial flux permanent magnet synchronous machine with housing-cooling," *IEEE Trans. Appl. Supercond.*, vol. 31, no. 8, pp. 1–5, Nov. 2021, doi: 10.1109/TASC.2021.3103728.

[18] H. Ding, W. Sixel, L. F. Handy-Cardenas, and B. Sarlioglu, "Investigation of the self-cooling characteristics of a novel flux-switching permanent magnet machine," in *Proc. IEEE Energy Convers. Congr. Expo. (ECCE)*, Sep. 2019, pp. 6562–6568, doi: 10.1109/ECCE.2019.8912946.

[19] H. Ding, W. Sixel, L. Zhang, A. Hembel, L. Handy-Cardenas, G. Nellis, and B. Sarlioglu, "Evaluation of the self-cooling performance of a flux-switching permanent magnet machine with airfoil-shaped rotor," *IEEE Trans. Ind. Appl.*, vol. 57, no. 4, pp. 3710–3721, Jul. 2021, doi: 10.1109/TIA.2021.3083242.

[20] H. Chuan, R. Burke, and Z. Wu, "A comparative study on different cooling topologies for axial flux permanent magnet machine," in *Proc. IEEE Vehicle Power Propuls. Conf. (VPPC)*, Oct. 2019, pp. 1–6, doi: 10.1109/VPPC46532.2019.8952185.

[21] M. Alatalo, S. T. Lundmark, and E. A. Grunditz, "Evaluation of three cooling concepts for an electric vehicle motor—3D models," in *Proc. Int. Conf. Electr. Mach. (ICEM)*, vol. 1, Aug. 2020, pp. 867–873, doi: 10.1109/ICEM49940.2020.9270757.

[22] L. Yan, Z. Dong, and S. Zhang, "Thermal analysis of a novel linear oscillating machine based on direct oil-cooling windings," *IEEE Trans. Energy Convers.*, vol. 37, no. 2, pp. 1042–1051, Jun. 2022, doi: 10.1109/TEC.2021.3118930.

[23] Q. Lu, X. Zhang, Y. Chen, X. Huang, Y. Ye, and Z. Q. Zhu, "Modeling and investigation of thermal characteristics of a water-cooled permanent-magnet linear motor," *IEEE Trans. Ind. Appl.*, vol. 51, no. 3, pp. 2086–2096, May 2015, doi: 10.1109/TIA.2014.2365198.

[24] G. Zhang, W. Hua, M. Cheng, B. Zhang, and X. Guo, "Coupled magnetic-thermal fields analysis of water cooling flux-switching permanent magnet motors by an axially segmented model," *IEEE Trans. Magn.*, vol. 53, no. 6, pp. 1–4, Jun. 2017, doi: 10.1109/TMAG.2017.2668845.

[25] P. Lindh, I. Petrov, A. Jaatinen-Värri, A. Grönman, M. Martinez-Iturralde, M. Satrustegui, and J. Pyrhönen, "Direct liquid cooling method verified with an axial-flux permanent-magnet traction machine prototype," *IEEE Trans. Ind. Electron.*, vol. 64, no. 8, pp. 6086–6095, Aug. 2017, doi: 10.1109/TIE.2017.2681975.

[26] P. Liang, F. Chai, K. Shen, and W. Liu, "Thermal design and optimization of a water-cooling permanent magnet synchronous in-wheel motor," in *Proc. 22nd Int. Conf. Electr. Mach. Syst. (ICEMS)*, China, Aug. 2019, pp. 1–6, doi: 10.1109/ICEMS.2019.8922510.

[27] W. Jiang and T. M. Jahns, "Coupled electromagnetic-thermal analysis of electric machines including transient operation based on finite-element techniques," *IEEE Trans. Ind. Appl.*, vol. 51, no. 2, pp. 1880–1889, Mar. 2015, doi: 10.1109/TIA.2014.2345955.
[28] W. Yu, W. Hua, J. Qi, H. Zhang, G. Zhang, H. Xiao, S. Xu, and G. Ma, "Coupled magnetic field-thermal network analysis of modular-spoke-type permanent-magnet machine for electric motorcycle," *IEEE Trans. Energy Convers.*, vol. 36, no. 1, pp. 120–130, Mar. 2021, doi: 10.1109/TEC.2020.3006098.
[29] C. Liu, G. Yu, Y. Xu, J. Zou, and L. Xiao, "Electromagnetic-thermal timesaving coupling analysis of a water cooling IPM machine for accurate prediction performance," in *Proc. 22nd Int. Conf. Electr. Mach. Syst. (ICEMS)*, Aug. 2019, pp. 1–5, doi: 10.1109/ICEMS.2019.8921542.
[30] B. Zhang, R. Qu, X. Fan, and J. Wang, "Thermal and mechanical optimization of water jacket of permanent magnet synchronous machines for EV application," in *Proc. IEEE Int. Electric Mach. Drives Conf. (IEMDC)*, May 2015, pp. 1329–1335, doi: 10.1109/IEMDC.2015.7409234.
[31] J. Yao, Y. Zhang, H. Wang, F. Zhang, and C. Gerada, "Effect of multi-size magnetic powder gradation on magnetic properties of novel composite magnetic materials for HSPMSM," *IEEE Trans. Transport. Electrific.*, vol. 8, no. 3, pp. 3594–3605, Sep. 2022, doi: 10.1109/TTE.2022.3149820.
[32] J. Yao, H. Wang, Y. Zhang, H. Zhang, and F. Zhang, "Magnetic properties analysis of novel composite magnetic materials for HSPMSMs," *IEEE Trans. Magn.*, vol. 58, no. 4, pp. 1–10, Apr. 2022, doi: 10.1109/TMAG.2022.3144190.
[33] H. Luo, Z. Xu, Y. Zhang, H. Zhang, Q. Yu, and F. Zhang, "Rotor electrical conductivity and eddy current loss analysis of high-speed permanent magnet machine with a novel composite rotor," *IET Electric Power Appl.*, vol. 16, no. 1, pp. 15–28, Jan. 2022, doi: 10.1049/elp2.12131.
[34] M. Abdi, A. Noureddine, and M. Ould-Rouiss, "Numerical simulation of turbulent forced convection of a power law fluid flow in an axially rotating pipe," *J. Brazilian Soc. Mech. Sci. Eng.*, vol. 42, no. 1, pp. 1–11, Jan. 2020, doi: 10.1007/s40430-019-2099-7.

HAO LUO received the B.S. degree from the Shenyang University of Technology, Shenyang, China, in 2016, where he is currently pursuing the Ph.D. degree in electrical engineering. He is also a Researcher with the Shenyang University of Technology. His research interest includes the design and analysis of high-speed machines.

YUE ZHANG (Member, IEEE) received the B.S. degree from the Shenyang University of Technology, Shenyang, China, in 2011, the M.S. degree from Zhejiang University, Hangzhou, China, in 2014, and the Ph.D. degree from Queen's University Belfast, Belfast, U.K., in 2018. He is currently a Professor with Shandong University, Jinan, China. His research interest includes the design and analysis of electrical machines.

HUIJUN WANG (Member, IEEE) received the M.S. degree in electrical engineering from the Shenyang University of Technology, Shenyang, China, in 2006, and the Ph.D. degree in electrical and mechatronics engineering from Kyungsung University, Busan, South Korea, in 2009. He is currently with Beihang University, Beijing, China. His research interests include motor design and drive systems.

GUANGWEI LIU (Member, IEEE) received the B.S., M.S., and Ph.D. degrees in electrical engineering from the Shenyang University of Technology, Shenyang, China, in 2005, 2008, and 2015, respectively. He is currently a Professor in electrical machines with the School of Electrical Engineering, Shenyang University of Technology. His major research interest includes permanent magnet electrical machines and its drive systems.

FENGGE ZHANG (Member, IEEE) received the B.S., M.S., and Ph.D. degrees in electrical engineering from the Shenyang University of Technology, Shenyang, China, in 1984, 1990, and 2000, respectively. His research and teaching interests include electromagnetic theory, dynamic simulation, magnetic field analysis, optimized design, and computer control technology of electrical machines.